

Evaporator Design for an Isokinetic Total Water Content Probe in a Naturally Aspirating Configuration

D.R. Buttsworth¹, C. Davison², J. D. MacLeod², J.W. Strapp³

¹Faculty of Engineering and Surveying

University of Southern Queensland, Toowoomba, Queensland, 4350 AUSTRALIA

²Institute for Aerospace Research, National Research Council
Ottawa, Ontario, K1A 0R6, CANADA

³Environment Canada, Downsview, Ontario, M3H 5T4, CANADA

Abstract

A number of recent aircraft turbofan power failure events have been linked to ice accretion in the initial compressor stages while the aircraft is traversing the anvil region of storm clouds. The water content in such cloud regions is not well known and the accuracy of most existing water content probes is likely to be poor under such conditions. A new cloud water content probe is being developed for airborne characterisation of such clouds and a critical feature of the probe is the evaporator. In this work we develop some analytical expressions to assist in the design and characterisation of the evaporator. In particular, we consider the issue of convective heat transfer to the ice and water particles moving with the air flow through the evaporator. For the particular evaporator design we are considering, it is shown that ice particles larger than 100 μm are unlikely to have sufficient residence time to evaporate if they remain suspended in the heated air. Although these larger ice particles are likely to impact on the evaporator walls so there is also an opportunity for direct conduction heating, the present analysis indicates that particles larger than 100 μm may not adhere to the walls. However, there are many uncertainties in the present analysis and experiments are needed to determine the actual performance of the evaporator.

Introduction

Extensive research on the dynamic region of storm systems has been already performed and interest has generally focussed on the lightning, rain, hail, and winds associated with these deep convective systems. However, little is known about conditions, and in particular the cloud water content, in the apparently benign but extensive outflow regions of these clouds. Pilots are normally able to avoid the regions of intense activity in storms which are normally displayed as a red echo region on their airborne radar signals. However, it is occasionally necessary for pilots to penetrate the extensive outflow regions, known as the anvil, due to flight path restrictions and prevailing weather conditions.

Until recently, traverses through the anvil have been considered safe. However, a number of recent turbofan power failure events in large transports and commuter aircraft have been linked to ice accretion on engine components during flight through apparently benign, high altitude clouds events [1,2]. Although the total water content in the anvil region of deep convective systems could be quite high, it is not identified as such on the airborne radar (a green echo is displayed in these regions) because the water content is in the form of ice which is not detected by the airborne radar frequency.

The type of 'icing' that seems to occur during flights through the anvil is quite different to the ice accretion from supercooled large droplet (SLD) conditions which is a well known problem and is covered extensively in existing regulations. In SLD icing conditions, the liquid particles impacting on aircraft become ice and the build-up of ice can be identified from visual inspection, icing detectors, and changes in aircraft handling.

However, when flying through anvil regions, ice does not appear to accrete on the aircraft external surfaces – there is no observable build up of ice on the wings and the aircraft handling does not change, nor is there any ice detection by the normally-reliable icing detectors. The ice seems to 'bounce' off the aircraft harmlessly suggesting there is no danger. However, it is possible for the ice to build up in stagnation regions of turbofan compressors (stators). This ice build up can lead to unsteady engine performance – compressor surge or stall, or perhaps an uncommanded power reduction from the engine. This so called engine 'rollback' seems to arise because of reduced compression efficiency associated with ice build up. Reduced compression efficiency leads to a rotor speed reduction which in turn allows further ice build up finally resulting in a steady state operating condition that is overheated at sub-idle with no response to commanded changes in throttle setting. It is also possible for the ice to suddenly release from the stator and be ingested into subsequent compressor stages perhaps causing any combination of surge, stall, and engine damage. Released ice can finally enter the combustion chamber possibly resulting in a flame out events [1,2].

A wide variety of cloud water content probes have already been developed but none appear well suited to conditions expected in the anvil of deep convective systems. For example, the Nevzorov total water content probe identifies water content from the thermal energy required to evaporate water particles captured within a conical surface [3]. However, under high water content conditions, ice and liquid water particles entering the probe have been observed to cause a loss of water content from the probe in both wind tunnel and flight experiments. Therefore, under high water content conditions the probe is expected to underestimate the cloud water content [4,5,6].

Overview of Probe Design

We are developing a new total water content probe which samples the cloud isokinetically – the volumetric flow rate entering the probe will ideally be equal to the open area of the probe tip multiplied by the speed of the aircraft on which the probe is mounted. The anticipated arrangement is illustrated in figure 1. Ice and water particles entering the probe will be evaporated and the total water content will be deduced using a hygrometer which samples the flow downstream of the

evaporator. The performance of the evaporator is therefore critical to the overall success of the probe. The design of the evaporator also requires special attention because of the limited electrical power available from the aircraft.

The new cloud TWC probe is similar to the device of Nicholls et al. [7] in that the probe is being designed for isokinetic operation in a naturally aspirating configuration, but we are aiming to quantify and control the inlet velocity through flow rate measurement and online adjustment of the downstream aperture if necessary to maintain optimal isokinetic performance. Experiments to date indicate that the diffuser, which is located just downstream of the probe intake, is performing as intended. There is sufficient pressure recovery in the diffuser to maintain isokinetic performance at the anticipated flight conditions.

In this paper we are primarily concerned with the design of the evaporator. The envisaged evaporator consists of a heated, coiled tube with a 1" internal diameter. At a flight speed of 200 m/s and an altitude of 10.5 km, the flow entering the evaporator is expected to have a pressure of 31 kPa, a temperature of 240 K, and a speed of 28 m/s.

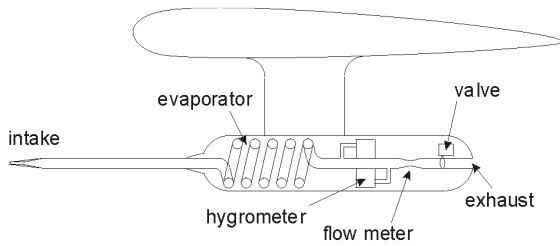


Figure 1. Overview of anticipated isokinetic probe arrangement showing a coiled-tube evaporator within the instrumentation canister.

Air to Particle Heat Transfer

Air entering the evaporator is heated convectively. Ice particles that remain suspended in the air flow will be convectively heated by the surrounding air. (Direct radiative heating of ice particles is insignificant due to the modest evaporator wall temperatures currently being considered.) Particles of ice and water suspended in the evaporator air are treated using an empirical correlation appropriate for spherical particles,

$$Nu = 2 + 0.6Re_{d_p}^{1/2} Pr^{2/3} , \quad (1)$$

where Nu is the Nusselt number, Re_{d_p} is the Reynolds number based on particle diameter d_p , and Pr is the Prandtl number.

To apply this correlation, the Reynolds number is needed and for this, the relative velocity between the particles and the surrounding air is required. Stokes' number (Stk), can be used to give an indication of the likely behaviour of aerodynamic particles and is given by

$$Stk = \frac{\tau_p}{\tau_f} , \quad (2)$$

where τ_p is an appropriate particle dynamics time scale, and τ_f is an appropriate flow time scale. For $Stk \ll 1$, the particle trajectory will be dictated largely by the local flow conditions and the particle should closely follow the flow streamlines whereas for $Stk \gg 1$, particle paths are not influenced by local flow conditions.

In the present case, we estimate τ_p on the assumption that Stokes' law for particle drag applies ($C_d = 24/Re$) resulting in the particle dynamics time scale (sometimes known as the "particle relaxation time") given by

$$\tau_p = \frac{\rho_p d_p^2}{18\mu} \quad (3)$$

Where ρ_p is the particle density and μ is the dynamic viscosity of the surrounding fluid (air, in the present application).

For turbulent flow through the curved evaporator tube, there are two flow time scales that are particularly relevant. The first time scale that we identify is the time taken by the mean flow to turn through 90 degrees. This is given by

$$\tau_{f1} = \frac{\pi R}{2U} \quad (4)$$

where R is the radius of curvature of the coiled-tube evaporator and U is the mean pipe flow speed. The second time scale that we identify is associated with the turbulent fluctuations. In the case of fully developed turbulent flow in a straight pipe, the intensity (u'/U) and length scale (l) of the turbulence can be estimated using

$$\frac{u'}{U} = 0.16 Re_D^{-1/8} , \quad (5)$$

and

$$l = 0.07 D , \quad (6)$$

where Re_D is the Reynolds number based on the pipe diameter D . Hence, we estimate the flow time scale using

$$\tau_{f2} = \frac{l}{u'} = 0.44 \frac{D}{U} Re_D^{1/8} . \quad (7)$$

For the evaporator design conditions currently being considered, $R = 80$ mm resulting in $\tau_{f1} = 4.48$ ms, and $Re_D = 16,300$ resulting in $\tau_{f2} = 1.37$ ms.

For $\tau_p \ll \tau_{f2}$ we expect the relative velocity u_{rel} between the ice particles and the surrounding air to approach zero – under these conditions the speed of the particles will rapidly adjust to the speed of the local turbulent fluctuations. For $\tau_p \approx \tau_{f2}$, the turbulent fluctuations should either accelerate or decelerate the particles depending on their initial speed so we assume $u_{rel} = 0.5 u'$ when $\tau_p = \tau_{f2}$. For larger particles sizes where $\tau_p \approx \tau_{f1}$ we expect the particles to collide regularly with the walls of the evaporator tube. The dynamics of such particles will primarily be influenced by the mean flow in the pipe and the tube walls so we take the relative velocity to be $u_{rel} = 0.5 U$ when $\tau_p \geq \tau_{f1}$.

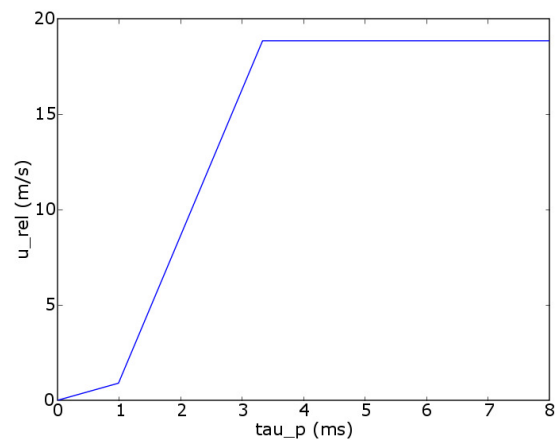


Figure 2. Assumed relationship between u_{rel} and τ_p at the present design conditions.

The resulting relationship between the relative velocity and the particle dynamics time scale is shown in figure 2 for the present design conditions. For values of $\tau_p > 4.48$ ms, the value of u_{rel}

plateaus at 18.8 m/s corresponding to half of the evaporator flow speed after the flow has been heated to 323 K.

Droplet Evaporation

To estimate the rate of droplet evaporation, we adopt the Chilton-Colburn analogy relating the heat transfer coefficient h (units of W/m²K) and the mass transfer coefficient k_c (units of m/s) according to

$$\frac{h}{k_c} = \rho c_p Le^{2/3}, \quad (8)$$

where ρ is the density, c_p is the specific heat at constant pressure, and Le is the Lewis number – all referring to the conditions in the air surrounding the evaporating particle (taking the surrounding fluid to be a dilute water vapour-air mixture that can be treated using air properties alone).

The rate of evaporation of water mass \dot{m} is then obtained from the mass transfer coefficient definition

$$\dot{m} = k_c A_p \rho (Y_s - Y_\infty), \quad (9)$$

where A_p is the surface area of the particle, Y is the mass fraction of the water vapour, and subscripts s and ∞ refer to conditions at the particle surface and in the far field. Taking $Y_\infty = 0$ (the dilute mixture approximation) and assuming k_c is independent of particle size, the time for evaporation can then be estimated using

$$t_{\text{evap}} = \frac{d_p \rho_l}{2k_c \rho Y_s}. \quad (10)$$

where ρ_l is the density of the liquid. Water vapour mass fraction at the surface of the particle (Y_s) is determined from the mixture equations relating mole and mass fractions and the mole fraction is determined from the vapour partial pressure taken as the saturation pressure of water at the particle temperature.

Particle Heat Transfer and Evaporation Results

The time needed to heat and evaporate particles of various diameters in the coiled pipe flow evaporator are presented in figure 3 (according to the models presented in sections Air to Particle Heat Transfer and Droplet Evaporation). For these calculations the ice particles are assumed to enter the evaporator at 220 K and the evaporator air is assumed to be heated (instantaneously) to 323 K.

The change in slope of the lines in figure 3 for particle diameters between about 19 and 36 μm corresponds to the change in relative velocity between the air and the particles that occurs for particle response times between 1.37 and 4.48 ms (as illustrated in figure 2). For convenience, evaporation was assumed to occur at a constant temperature of 45 °C and this degree of approximation is consistent with other aspects of the heat transfer modelling. Obviously evaporation will start before the droplets reach 45 °C and heat transfer will continue after the droplets reach 45 °C – both effects tending to make the current estimate of evaporation time longer than it would be in reality.

If the coiled tube evaporator is configured with an overall length of about 4 m, the residence time at the design conditions would be about 100 ms. Hence particles larger than 100 μm are unlikely to have sufficient time to evaporate because of air to particle heat transfer, figure 3. However, these larger diameter particles are actually more likely to interact with the evaporator tube walls than the small particles since their particle dynamics time scales are larger than the mean, coiled tube flow time scale. Thus, there will be an opportunity for these particles to be heated directly from the evaporator walls, rather than relying entirely on heat transfer from the heated air. The interaction of ice particles and the evaporator surface is considered in subsequent sections.

A lumped heat capacity analysis was adopted for the transient heat transfer calculations (results of which are presented in figure 3) and this is appropriate since the Biot numbers for the present conditions ranged from 0.03 (for the 1 μm particles) to 0.17 (for the 1 mm particles). These Biot numbers imply that the lumped capacity approach is valid for all sized particles considered, and that the temperature throughout each particle is essentially uniform. Thus, water is unlikely to develop at the surface of the ice particles while suspended in the air flow unless the particles are already approaching their melting point.

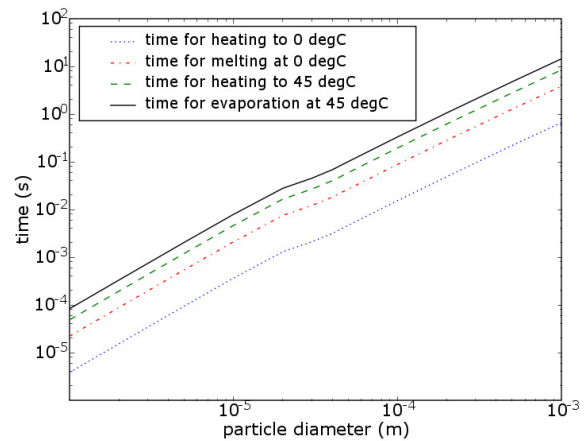


Figure 3. Calculated heating and evaporation times for particles diameters from 1 μm to 1 mm.

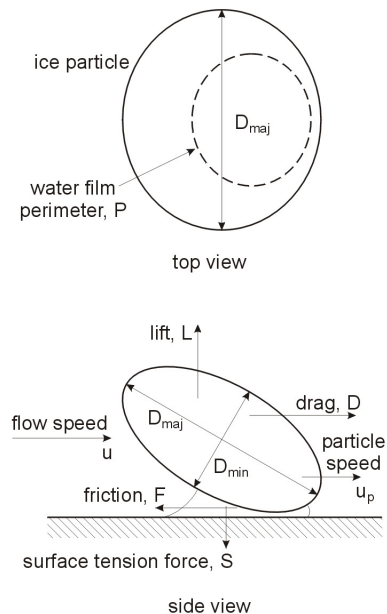


Figure 4. Illustration of model for forces on an ice particle adhering to the surface via a water film.

Water Film Development

The presence of a water film can dramatically alter the dynamics of ice particles during a collision with a wall or other particles. As noted previously, a water film is unlikely to develop around an ice particle while suspended in the air. However, a water film may develop during collision with a heated wall.

When two objects at different initial temperatures are suddenly brought into contact, the interface of each object will adopt the same intermediate temperature, neglecting any thermal contact resistance. Assuming the ice particles and the evaporator wall can be treated as thermally semi-infinite on the time scales of interest for the impact event, the interface between the ice and the wall will have a temperature given by

$$T_{\text{interface}} = \frac{T_{\text{ice}} + \beta T_{\text{wall}}}{1 + \beta} \quad (11)$$

where

$$\beta = \frac{(\sqrt{\rho c k})_{\text{wall}}}{(\sqrt{\rho c k})_{\text{ice}}} \quad (12)$$

and ρ , c , and k are the density, specific heat and thermal conductivity respectively.

Rearranging equation 11, we have

$$T_{\text{wall}} = \frac{T_{\text{interface}} - T_{\text{ice}}}{\beta} + 1 \quad (13)$$

Assuming there is sufficient time during the impact event for changes in molecular structure, a water film will develop at the surface of the ice particle provided $T_{\text{interface}} > 273$ K. (Depending on the contact pressures between the ice and the wall, the local ice melting point may be lowered by several degrees.) Hence the limiting evaporator wall temperature for development of a water film can be written

$$T_{\text{wall}} (^{\circ}\text{C}) > \frac{-T_{\text{ice}} (^{\circ}\text{C})}{\beta} \quad (14)$$

For a typical aluminium alloy, $\beta \approx 11$ and for copper, $\beta \approx 19$. Thus, for ice particles at -50 $^{\circ}\text{C}$, the minimum evaporator surface temperature required for generation of water during impact will be about 4.5 $^{\circ}\text{C}$ in the case of an aluminium evaporator, and 2.6 $^{\circ}\text{C}$ in the case of a copper evaporator. We expect to operate the evaporator at temperatures well above these values and hence there are good prospects for the formation of a water film at the points of contact on the ice particles.

Adhesion of Ice Particles to Surface

If surface adhesion of ice particles occurs, it should improve prospects for melting and evaporating particles that do not have sufficient residence time to evaporate due to heat transfer from the air alone. Assuming a water film exists between the ice particle contact points and the surface, we expect that the particles will remain attached to the surface provided the water surface tension force S (acting perpendicular to the evaporator surface) is not exceeded by the lift force L . That is, the condition for particle attachment can be written

$$L \leq S. \quad (15)$$

The surface tension force can be written in terms of the surface tension σ and perimeter of water P that adheres the ice particle to the surface

$$S = \sigma P. \quad (16)$$

The lift force on the ice particle can be written in terms of the coefficient of lift C_L , the reference area for the lift coefficient A , and the dynamic pressure

$$L = C_L \frac{1}{2} \rho (u - u_p)^2 A, \quad (17)$$

where ρ is the flow density, u is the local flow velocity, and u_p is the particle velocity in the downstream direction.

Assuming the ice particles are approximately oblate spheroids, we can adopt the experimental values of C_L obtained by List et al. [8] as reported in Table 1. For Reynolds numbers (based on the major axis length) between 40×10^3 and 200×10^3 , List et al. [8] found the aerodynamic coefficients were largely independent of

Reynolds number. In table 1, the reference area of the lift coefficient C_L and drag coefficient C_D is

$$A = \pi D_{\text{maj}}^2 / 4, \quad (18)$$

where D_{maj} is the major axis length and the angle of attack α is defined angle of inclination of the minor axis relative to undisturbed flow direction. The coefficient of lift reaches a maximum value of about 0.3 for angle of attack of 45° for axis ratio of 0.5.

α	$D_{\text{min}}/D_{\text{maj}}$	C_L	C_D
0	0.5	0	0.8
15	0.5	0.18	0.74
45	0.5	0.3	0.52
75	0.5	0.25	0.20
90	0.5	0	0.17
45	0.6	0.23	--
45	0.8	0.15	--
0	0.8	0	0.63
90	0.8	0	0.39

Table 1. Aerodynamic coefficients for oblate spheroids with axis ratios between 0.5 and 0.8 from [8] for $40 \times 10^3 < \text{Re} < 200 \times 10^3$.

In the case of a fully developed turbulent pipe flow, the flow velocity in the vicinity of a small particle adhering to the wall can be estimated using

$$u = \frac{D_{\text{maj}}}{2} \frac{u_*^2}{\nu} \quad (19)$$

where

$$u_*^2 = \frac{1}{8} f U^2 \quad (20)$$

And ν is the kinematic viscosity. With this approach we are assuming the particle remains within the viscous sublayer and that the appropriate local velocity is the undisturbed boundary layer velocity at a distance from the surface corresponding to half of the particle's major diameter. For a turbulent flow in a coiled tube, we estimate the friction factor using

$$f = \frac{0.336}{\text{Re}_D^{0.2} \left(\frac{D}{2R} \right)^{0.1}}. \quad (21)$$

The above correlation is presented by Blevins [9] for coiled tube flow at conditions close to those expected in the present arrangement. If we now assume

$$u_p \ll u, \quad (22)$$

and that the perimeter of water that adheres the particle to the surface scales with the major diameter of the particle

$$P = n \pi D_{\text{maj}}, \quad (23)$$

where n is some constant with a likely magnitude less than 1, then we can combine the above equations with the condition for particle attachment to obtain

$$U \leq 21.55 \left[\frac{n \sigma}{C_L} \right]^{0.278} \frac{\nu^{0.444} D^{1.667}}{\rho^{3.6} R^{0.0556}} \frac{1}{D_{\text{maj}}^{0.833}}. \quad (24)$$

Frictional Deceleration of Particles at Surface

If the friction acting on an ice particle during a glancing collision with the wall of the evaporator exceeds the drag on the particle, then the particle should decelerate, thereby improving prospects for development of an extensive water film and enhancing adhesion. Conversely, an ice particle that accelerates along the wall because the drag force exceeds the friction is expected to partially shed its water film so prospects for continued adhesion will diminish.

If the friction force F on an ice particle attached to, and moving along the surface exceeds the aerodynamic drag D on the particle, then the particle will decelerate. The condition for particle deceleration can be written

$$D < F. \quad (25)$$

In the same way as the lift force discussed in the previous section, the drag force can be identified if we can estimate the drag coefficient

$$D = C_D \frac{1}{2} \rho (u - u_p)^2 A. \quad (26)$$

The friction force can be estimated from the net downwards normal force and the coefficient of friction μ_f using

$$F = \mu_f (S - L). \quad (27)$$

Adopting similar approximations and simplifications used in the previous section we can write the condition for ice particle deceleration as

$$U < 21.55 \left[\frac{n\sigma}{C_L + C_D / \mu_f} \right]^{0.278} \frac{\nu^{0.444} D^{1.667}}{\rho^{3.6} R^{0.0556}} \frac{1}{D_{maj}^{0.833}} \quad (28)$$

Adhesion and Deceleration Results

The limiting pipe flow velocities for particle adhesion and deceleration as identified from equations 24 and 28 are presented in figure 5. Combinations of particle diameters and evaporator pipe flow speeds that lie below the lines in figure 5 are likely to result in particle deceleration and/or adhesion, while for points lying above the lines in figure 5, deceleration and/or adhesion is unlikely to occur.

For these calculations we assumed ice particles were oblate spheroids with an axis ratio of 0.5 and an angle of attack of 45°, in which case appropriate estimates of C_L and C_D are 0.30 and 0.52 respectively (table 1). Air properties (viscosity and density) were evaluated at 31 kPa and 50 °C, and the evaporator internal diameter was $D = 0.0254$ m and the coil radius of curvature was $R = 0.08$.

Water surface tension was taken as $\sigma = 0.0755$ N/m (appropriate for temperatures approaching freezing), and the coefficient of friction of the ice was taken as, $\mu_f = 0.02$. The coefficient of friction for ice is likely to be a function of the thermal properties of the surface, the temperature, and relative speed between the ice and the surface as demonstrated in the work of Evans et al. [10]. However, the value of 0.02 is representative of the values obtained by Evans et al. [10] and assuming such a constant value is consistent with the level of approximation necessary elsewhere in this work.

The perimeter of the water film between the ice particle and the evaporator surface is a source of large uncertainty in the current analysis. In the above adhesion and deceleration models, it was assumed the total perimeter of the water film would scale with the particle diameter, but this scaling is not certain. The picture of a continuous water film between the particle and wall (figure 4) is unrealistic for the initial particle-wall impact event. Immediately following impact, it is more likely that a number of water films will develop at the local points of contact between the ice particle and the wall. To make modelling improvements in this area, knowledge of the likely surface topology of the ice particles is required.

Nevertheless, proceeding on the assumption that the water film perimeter is n times the particle circumference (around the major diameter) as indicated in equation 23, results are presented in figure 5 for the deceleration condition with $n = 0.01, 0.1, \text{ and } 1$, and for the adhesion condition with $n = 1$. (It seems likely that

low values of n would apply during the initial stages of particle-surface interaction.) Comparison of the adhesion and deceleration conditions (equations 24 and 28, and figure 5) indicates that if a particle decelerates, it will also adhere to the surface, but that adhering particles may or may not decelerate, depending on the flow speed.

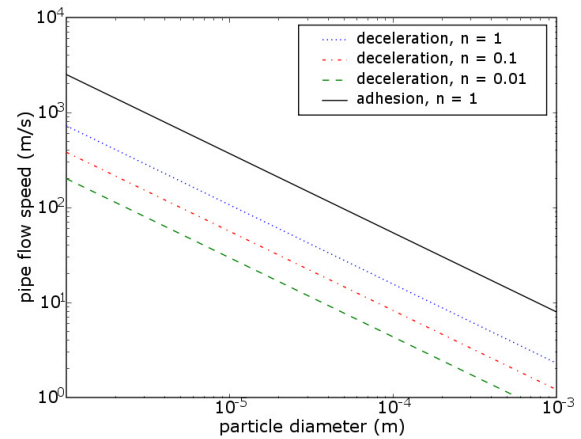


Figure 5. Limiting pipe flow speed for surface adhesion and deceleration of particles with diameters from 1 μm to 1 mm.

Particles larger than about 100 μm are unlikely to have sufficient residence time to melt and evaporate if they remain suspended in the air stream (figure 3), so the current evaporator design concept relies on the heating of these particles via direct contact with the evaporator walls. The present analysis (figure 5) indicates that at a pipe flow speed of 37.7 m/s (the anticipated evaporator flow speed when the air is heated to 50 °C), particles larger than 100 μm will not decelerate since the point (100 μm , 37.7 m/s) falls above the $n = 1$ deceleration line. Furthermore, particles larger than 100 μm may also have difficulty adhering because a relatively large film perimeter of film is required ($n = 0.27$) for a 100 μm particle to adhere in a 37.7 m/s pipe flow.

Application to Analysis of Ice Accretion

Conditions that favour particle deceleration and adhesion are advantageous for ice melting and evaporation only if the heat transfer from the surface is high enough. If the heat transfer from the surface to the particles is modest and/or the number of particles is high, flow and surface conditions that favour particle deceleration and adhesion will be likely to cause ice accretion.

The deceleration and adhesion analysis introduced previously was in the context of the design of a turbulent, coiled pipe flow evaporator. This analysis can be adapted to the case of flow in the vicinity of a stagnation region such as is relevant to the case of ice accretion in turbofan compressors. The elements missing from the previous analysis that are necessary for the problem of ice accretion modelling include: (i) the analysis of the heat transfer from the surface to the particle; (ii) the subsequent melting and evaporation of the water while in contact with the surface; and (iii) and the probability of subsequent ice particle impacts prior to complete evaporation.

Conclusions

The present analysis suggests the melting and evaporation of ice particles smaller than 100 μm should be readily accomplished by the current evaporator design. However, particles larger than 100 μm will not have sufficient residence time to evaporate if they remain suspended in the air stream, and even when they collide with the walls of the evaporator, adhesion of the ice to the

evaporator walls is not certain. However, there are many assumptions and uncertainties in the current analysis including the shape and orientation of the ice particles and the perimeter of the water film. Tumbling motion of the ice particle is also ignored. Experiments are needed in order to determine the performance and define the operating limits of the planned evaporator configuration.

Acknowledgments

DRB thanks USQ for approving leave for him to work at the National Research Council (NRC) in Ottawa and the NRC for hosting his visit in July and August, 2007.

References

- [1] Lawson, R.P., Angus, L.J., & Heymsfield, A.J., Cloud Particle Measurements in Thunderstorm Anvils and Possible Weather Threat to Aviation, *J. Aircraft*, **35**, 1, 1998, 113-121.
- [2] Mason, J.G., Strapp, J.W., & Chow, P., The ice Particle Threat to Engines in Flight, AIAA Paper 2006-206, 44th AIAA Aerospace Sciences Meeting and Exhibit, 9-12 January 2006, Reno, Nevada.
- [3] Korolev, A. V., Strapp, J. W., Isaac, G. A., Nevzorov, A. N., The Nevzorov Airborne Hot-Wire LWC-TWC Probe: Principle of Operation and Performance Characteristics, *Journal of Atmospheric and Oceanic Technology*, **15**, 1998, 1495-1510.
- [4] Miller, D. R., Lynch, C. J., Tate, P. A., Overview of High Speed Close-Up Imaging in an Icing Environment, AIAA Paper 2004-0407, 42nd AIAA Aerospace Sciences Meeting and Exhibit, 5-8 January 2004, Reno, Nevada. Also available as NASA/TM-2004-212925, Feb 2004.
- [5] Emery, E., Miller, D., Plaskon, S. Strapp, J. W., Lillie, L. E., Ice Particle Impact on Cloud Water Content Instrumentation, AIAA Paper 2004-0731, 42nd AIAA Aerospace Sciences Meeting and Exhibit, 5-8 January 2004, Reno, Nevada. Also available as NASA/TM-2004-212964, March 2004.
- [6] Isaac, G. A., Korolev, A. V., Strapp, J. W., Stewart, G. C., Boudala, F. S., Marcotte D., Reich, V. L., Assessing the Collection Efficiency of Natural Cloud Particles Impacting the Nevzorov Total Water Content Probe, AIAA Paper 2006-1221, 44th AIAA Aerospace Sciences Meeting and Exhibit, 9-12 January 2006, Reno, Nevada.
- [7] Nicholls, S., Leighton, J., and Barker, R. A new fast response instrument for measuring the total water content from aircraft, *J. Atmospheric and Oceanic Technology*, **7**, 1990, 706 – 718.
- [8] List, R., Rentsch, U.W., & Byram, A.C., On the Aerodynamics of Spheroidal Hailstone Models, *J. Atmospheric Sciences*, **30**, 1973, 653-661.
- [9] Blevins, R.D., Applied Fluid Dynamics Handbook, Krieger Publishing Company, Malabar, Florida, 1992.
- [10] Evans, D.C.B., Nye, J.F., Cheeseman, K.J., The Kinetic Friction of Ice, *Proc. R. Soc. Lond.*, A **347**, 1976, 493-512.